# Relationship Between Crystalline Structure and Mechanical Behavior in Isotropic and Oriented Polyamide 6

**Nadya Dencheva,[1] Zlatan Denchev,[1] M. Jovita Oliveira,[1] Sérgio S. Funari[2]**

[1]*Institute for Polymers and Composites, Department of Polymer Engineering, University of Minho, 4800-058 Guimarães, Portugal*
[2]*HASYLAB at DESY, Notkestraße 85, 22603 Hamburg, Germany*

Received 6 July 2006; accepted 7 August 2006
DOI 10.1002/app.25250
Published online in Wiley InterScience (www.interscience.wiley.com).

**ABSTRACT:** Polyamide 6 (PA6) isotropic films and oriented cables were prepared by compression molding or by consecutive extrusion and cold-drawing. These samples were isothermally annealed in the 120–200°C range and were then subjected to tensile tests at room temperature. Synchrotron wide-angle X-ray scattering (WAXS) and small-angle X-ray scattering (SAXS) patterns were obtained before and after mechanical failure. These data were related with the mechanical properties of the respective PA6 samples. The annealing of isotropic PA6 resulted in an increase in the Young's modulus ($E$) and yield stress ($\sigma_y$) values, which was attributed to the observed proportional reduction of the $d$-spacings of the intersheet distances in both the α-PA6 and γ-PA6 polymorphs. Analysis of the WAXS and SAXS patterns of isotropic PA6 after break allowed the supposition of structural changes in the amorphous phase, with these being better pronounced with increasing annealing temperature; this made the samples less ductile. In oriented PA6 samples, annealing resulted in a drastic increase in the $E$ and $\sigma_y$ values accompanied by a phase transition from γ-PA6 to α-PA6 and a well-pronounced reduction in the intersheet distances of both polymorphs. The stretching of the oriented samples led to an additional γ-to-α transition, whose extent was also related to structural changes in the amorphous phase. © 2006 Wiley Periodicals, Inc. J Appl Polym Sci 103: 2242–2252, 2007

**Key words:** mechanical properties; polylactams; polymorphism; SAXS; WAXS

## INTRODUCTION

Of all the *n*-polyamides currently known and manufactured on an industrial scale, polyamide 6 (PA6) has achieved the widest commercial use and is the best studied. The processing of PA6 may be divided into three broad categories: melt spinning, extrusion, and injection molding. The end products are various types of yarns, films, sheets, rods, tubes, coatings of electric conduits, and so on.[1] A recent application of PA6 is a reinforcing component in what are called *microfibrillar in situ composites*.[2,3] All of these processing techniques comprise controlled heat and/or mechanical treatments that have an important impact on the PA6 crystalline structure and, hence, on its mechanical properties.

Although there are a large number of studies relating the structure or the properties of PA6 to the conditions of its orientation and annealing, relatively few works have been published so far on the relationship between the mechanical properties and crystalline structure. Galeski et al.[4] studied the mechanisms of deformation of PA6 in uniaxial extension by means of X-ray, microscopy, and calorimetric techniques. The stretching of PA6 reportedly led to the orientation of the α and γ crystals with macromolecular chains parallel to the drawing direction. It was also demonstrated that the α phase experienced a larger amount of breakdown between the planes determined by the hydrogen bonds compared to the γ phase. In plane-strain compression mode, Gasleski et al.[5] also observed a share-induced α-to-γ transition, which created small amounts of γ polymorph in the originally all-α-form crystalline phase. The latter underwent extensive deterioration by a chain-slip mechanism along the (002) planes containing the hydrogen bonds.

More recently, Lin and Argon[6] performed extensive structural and mechanical investigations on plastic deformation in PA6 by means of X-ray scattering and electron microscopy. Quasisingle crystal PA6 samples were prepared by plain-strain compression at an elevated temperature in a channel die. Investigation of the crystallographic slip processes confirmed the con-

*Correspondence to:* Z. Denchev (denchev@dep.uminho.pt).
Contract grant sponsor: European Commission; contract grant number: IHP HPRI-CT-2001-00140 and HASYLAB Project II-04-047 EC.
Contract grant sponsor: Fundaçâo para a Ciência e Tecnologia (FCT); contract grant number: POCI/CTM/57358/2004.
Contract grant sponsor: Fundação para a Ciência e Tecnologia, Portugal; contract grant number: SFRH/BD/13435/2003 (to N.D.).

clusion that in the more stable α form, the (002) planes of the H-bonded sheets constituted the main active slip system. Lin and Argon[7] also presented an interesting analysis of the crystal slip thermal activation.

Ito et al.[8] investigated the effects of the PA6 α and γ crystalline forms on deformation behavior. α-PA6 crystals were obtained from solution or melt under ordinary crystallization conditions. The α phase was converted into the γ form by iodine treatment. Wide-angle X-ray scattering (WAXS) and small-angle X-ray scattering (SAXS) techniques were used for structural characterization, and dynamic mechanical analysis was used to study the mechanical properties. The general conclusion was that the γ form was more ductile than the α form. However, the authors did not elucidate the potential influence on ductility of the profound chemical changes of the γ-PA6 phase studied.

The mechanical behavior and structural evolution on uniaxial and biaxial drawing above the glass-transition temperature of PA6 films was studied in detail by Penel-Pierron et al.[9] by means of WAXS, infrared spectroscopy, and differential scanning calorimetry. The authors observed a higher ductility of PA6 in what they called the *mesomorphic* β *form* compared to samples in the γ and α forms. Under uniaxial drawing, a greater part of the β phase was shown to undergo strain-induced transition into α-PA6, with the latter being more pronounced above 120°C. The γ phase, which was thermally stable up to 200°C, also transformed into α-PA6. A structural explanation for the improved ability of PA6 for biaxial orientation at temperatures below 120°C was presented. It was related to the β → α phase reorganization at higher temperatures accompanied by a collapse of the van der Waals interactions between the sheets, which led to sample splitting under normal stress conditions.

This article is a part of a broader study on the structure–properties relationship in *in situ* composite materials based on polymer blends containing polyamides. We report on the mutual relationship between the crystalline structure and the mechanical behavior in well-characterized oriented or isotropic PA6 samples containing different amounts of α and γ polymorphs. The main goal of this study was twofold: (1) to investigate the influence of the starting structure (i.e., degree of crystallinity, content of α and γ polymorphs, and orientation) on the mechanical properties of the samples [e.g., Young's modulus ($E$), yield stress ($\sigma_y$) and elongation, at break ($\sigma_{br}$), elongation at break] and (2) to elucidate the impact of strain on the crystalline structure after sample failure with changes in the crystalline phase taken into consideration. For this purpose, synchrotron WAXS and SAXS patterns were obtained before and after mechanical failure of various PA6 samples and processed to extract information related to the crystallinity, $d$-spacings, long spacings ($L$'s), and phase transitions. An attempt was made to associate the WAXS and SAXS structural data with the mechanical properties of the samples.

## EXPERIMENTAL

### Materials and sample preparation

Ultramid B35 (BASF, Ludwigshafen, Germany), a medium-viscosity, general-purpose polycaproamide grade with a melting temperature of 220°C (differential scanning calorimetry) obtained by ring-opening polymerization, was used as a starting material. Two types of samples were prepared and studied. The first one, designated as PA6 film, was obtained by the compression molding of as-supplied granules; it was preliminarily dried for 5 h at 90°C. The starting material was pressed at 250°C, and a pressure of 6 tons was applied for 5 min, which was followed by isothermal crystallization for 1 h at three different temperatures: 120, 160, and 200°C. The 200–250 μm-thick films so prepared were cooled to room temperature at a rate of about 20°C/min. Five specimens for tensile stress measurements with lengths of 25 mm and widths of 4 mm were cut out of each film.

The second sample, designated as PA6 oriented cable, was prepared in an extruder line including a Lestritz LSM 30.34 (Nümberg, Germany) intermeshing corotating twin-screw extruder, two water baths, two haul-off units, and a winder positioned downstream. The extrusion was performed at a set temperature of 250°C. The extrudate was cooled in the first water bath to 12°C and drawn at a draw ratio (DR) of $\lambda = 2.6$. The final drawing was performed in the second haul-off unit after the stretched cable was heated to 90–96°C in the second water bath. More details about the extruder line can be found elsewhere.[2] The oriented PA6 cables were annealed with free ends at 120, 160, or 200°C in an oven. Each annealing temperature was reached at a heating rate of 10°C/min. After 1 h of annealing at the respective temperature, the heating was switched off, and the sample was cooled at about 10°C/min until it returned to room temperature. Five specimens with a gauge length of 50 mm were cut out of each PA6 cable for tensile testing.

### WAXS and SAXS measurements

Synchrotron radiation with a wavelength of 0.15 nm generated at the Soft Condensed Matter Beamline (A2) of HASYLAB (Hamburg, Germany) was used. The first setup used permitted two-dimensional (2D) SAXS and one-dimensional (1D) WAXS measurements. The sample-to-detector distance for SAXS was set to 2850 mm, with the diffraction patterns registered by means of a MARCCD 2D detector with exposure times between 30 and 90 s. The 1D WAXS profiles were registered by a linear scintillation detector positioned at 240 mm in respect to the sample holder.

In the second setup for 2D WAXS, the linear detector was removed, and the MARCCD detector was positioned 90 mm from the sample. A specially designed sample holder was used to allow controlled heating and cooling of the sample in the 25–300°C range. A multichannel process and program controller was used to regulate the sample temperature in heating or cooling at various rates. The difference between the readout and real temperature of the sample was 1–2°C at a heating or cooling rate of 20°C/min.

### SAXS and WAXS data handling

Corrections for background scattering, irradiated volume, and beam intensity were performed for each image. The 2D SAXS patterns were integrated in the range of scattering vector (**s**) values between 0 and 0.19 $nm^{-1}$; the modulus of **s** is defined as $\mathbf{s} = (\mathbf{s}_{12}^2 + \mathbf{s}_3^2)^{0.5} = (2/\lambda) \sin\theta$, being the scattering angle. For all isotropic samples, the 1D correlation function (CF) was calculated after Lorentz correction of the raw SAXS profiles, as indicated earlier.[10]

The 1D WAXS curves were also corrected for background scattering, irradiated volume, and beam intensity. Their scattering angle axis was calibrated with the angular position of the reflections of a standard crystalline poly(ethylene terephthalate) sample. The **s** range covered in the WAXS measurements was 0.3–4.8 $nm^{-1}$. All WAXS curves were fitted with Gaussian peaks. For the isotropic PA6 samples, the total degree of crystallinity [or crystallinity index (CI)] was calculated as a relation of the areas of all crystalline peaks to the total area underneath the WAXS curve:

$$\mathrm{CI} = \frac{\sum A_c}{\sum (A_c + A_a)} \quad (1)$$

where $A_c$ is the integrated area underneath the respective crystalline peaks and $A_a$ is the integrated area of the amorphous halo.

In the PA6 oriented cables, the intensity of the meridional pointlike reflections could not be determined from the 1D WAXS curves. In this case, $\Sigma A_c$ in eq. (1) measures the scattering intensity along the equator only; that is, one can define it as the equatorial crystallinity index (ECI).[10]

The 1D WAXS patterns were used also to determine the interplanar spacings ($d_{h00}$ and $d_{00l}$) with Bragg's law:

$$2d_{hkl} \sin\theta_{hkl} = \lambda \quad (2)$$

where $\lambda = 1.5$ Å is the X-ray wavelength and $\theta$ is half of the $2\theta$ position of the center of the respective crystalline peak. The $d$-spacing of the ($0k0$) crystalline planes was determined by the slicing of the meridional pointlike reflections of the 2D WAXS patterns of the oriented PA6 samples.

### Tensile tests

Uniaxial tensile tests were performed in an Instron (High Wycombe, UK) model 4505 tensile testing machine. The tests were carried out at 23 ± 2°C with a standard tensile force of 1 kN at constant crosshead speed of 50 mm/min. The nominal stress was determined as a ratio of the tensile force and the initial cross-section of the sample. The nominal strain was determined as a ratio of the sample gauge length at any time during drawing to that before drawing.

## RESULTS

### Mechanical data

Figure 1 shows the stress–strain curves of differently annealed isotropic PA6 films [Fig. 1(a)] and oriented cables [Fig. 1(b)]. All data extracted from these curves are presented in Table I.

Isotropic PA6 samples displayed an augmentation (from 40 to 50 MPa) of $\sigma_y$ as the temperature of annealing increased, accompanied by a statistically significant growth in $E$. At the same time, the strain dropped (Table I).

The oriented PA6 samples demonstrated different stress–strain curves on annealing [Fig. 1(b), Table I]. All samples showed two yield points, with the first being in the range between 66 MPa (cable without annealing) and 105 MPa (1 h at 160°C) and the second yield point being between 123 MPa (cable without annealing) and 180 MPa (1 h at 200°C). After the second yield point, strain hardening occurred; this was better observable in the sample without annealing. This same sample showed the biggest strain at break ($\varepsilon_{br}$). As with the isotropic films, an increase in the annealing temperature led to a significant drop in the strain values, whereby the sample annealed at 200°C showed almost brittle failure. At the same time, $E$ displayed an increase of more than three times and attained its maximum of 3.8 GPa for the sample heated at 200°C (Table I).

### 1D WAXS

1D WAXS patterns were obtained for isotropic (Fig. 2) and oriented (Fig. 3) PA6 samples initially annealed for 1 h at different temperatures in the 100–200°C range before and after tensile testing. After the curves were fitted as indicated earlier,[10,11] the data on the $\alpha$ and $\gamma$ crystal fractions, as well as of the total CIs, were obtained (Table II). In isotropic PA6 samples, the $\alpha$ form was the predominant one, and annealing in the

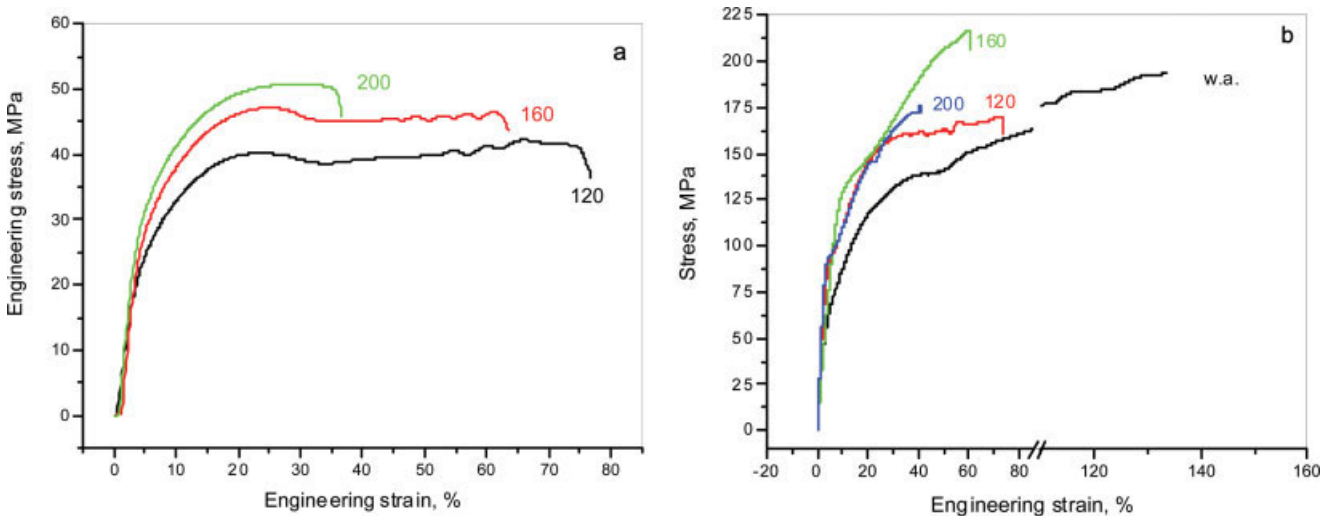


**Figure 1** Stress–strain curves of various PA6 samples: (a) isotropic films annealed for 1 h at 120, 160, or 200°C and (b) oriented PA6 cables without annealing (w.a.) and annealed at 120, 160, and 200°C for 1 h. The curves represented were selected to best fit the averaged data in Table II. [Color figure can be viewed in the online issue, which is available at www.interscience.wiley.com.]

120–200°C range did not significantly change the relation between the two polymorphs. The respective CI values remained between 44 and 45%. Stretching until mechanical failure of these samples led to an increase in α-CI, which was better expressed for the sample annealed at 120°C (by 10%). The γ crystalline fraction before and after sample failure remained unchanged or dropped slightly at the lowest annealing temperature.

Figure 3(a) and Table II confirm our previous finding[10] that oriented PA6 cables obtained by cold drawing to a high DR resulted in a crystalline structure containing more γ crystalline form than α crystalline form (33 vs 12%, respectively). Annealing of such cable in the 120–160°C range decreased the γ-phase content 2–5 times, whereas the α-type crystallinity grew at a similar rate. After 1 h at 200°C, this tendency inversed, with a slight decrease in the α-phase content. When an external tensile stress was applied to the oriented cable without annealing, this led to additional transformation of the γ form to the α form. As shown in Table II, the γ-PA6 fraction decreased from 33 to 16%, whereas the α-phase content grew from 12 to 32%. A similar trend was registered with the oriented PA6 samples annealed at 120 and 160°C. Stressing the sample annealed at 200°C caused the inverse transition: the γ-CI value on sample failure was more than 10% higher than before the tensile test. At the same time, α-CI decreased by 6%.

**TABLE I**
**Mechanical Properties of Isotropic and Oriented PA6 Samples After Various Annealing Procedures**

| Sample | Annealing temperature and time | $E$ (GPa) | $\sigma_y$ (MPa)[a] | Yield strain (%) | Maximum stress (MPa) | Maximum strain (%) | $\sigma_{br}$ (MPa) | $\varepsilon_{br}$ (%) |
|---|---|---|---|---|---|---|---|---|
| Isotropic PA6 | 120°C for 1 h | 0.73 ± 0.02 | 42 ± 2 | 24 ± 2 | 44 ± 3 | 66 ± 18 | 17 ± 8 | 81 ± 18 |
| Isotropic PA6 | 160°C for 1 h | 1,01 ± 0.04 | 47 ± 2 | 24 ± 3 | 47 ± 4 | 24 ± 3 | 30 ± 14 | 70 ± 18 |
| Isotropic PA6 | 200°C for 1 h | 1.03 ± 0.04 | 51 ± 2 | 28 ± 3 | 51 ± 2 | 28 ± 5 | 41 ± 12 | 37 ± 6 |
| Oriented PA6 | No annealing | 0.99 ± 0.04 | 66 ± 2<br>123 ± 2 | 42 ± 14 | 201 ± 17 | 149 ± 26 | 193 ± 16 | 150 ± 68 |
| Oriented PA6 | 120°C for 1 h | 1.78 ± 0.12 | 88 ± 1<br>157 ± 2 | 36 ± 3 | 169 ± 19 | 72 ± 20 | 169 ± 19 | 74 ± 20 |
| Oriented PA6 | 160°C for 1 h | 3.18 ± 0.14 | 105 ± 2<br>170 ± 3 | 28 ± 5 | 223 ± 14 | 62 ± 13 | 223 ± 16 | 64 ± 14 |
| Oriented PA6 | 200°C for 1 h | 3.78 ± 0.17 | 103 ± 3<br>180 ± 2 | 25 ± 3 | 185 ± 9 | 47 ± 9 | 185 ± 9 | 48 ± 10 |

Five standard specimens were analyzed for each sample.
[a] Oriented cables displayed two yield points.

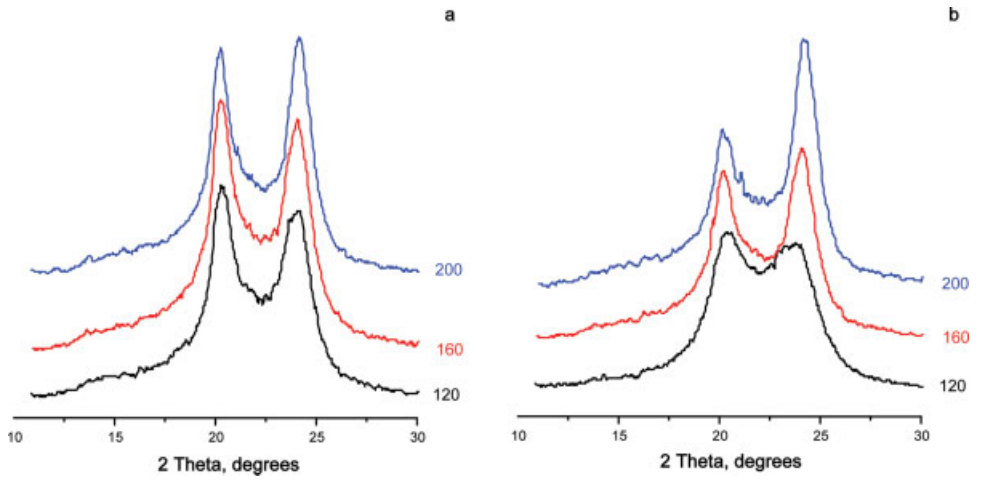


**Figure 2** 1D WAXS curves of isotropic PA6 films with annealing for1 h at different temperatures (a) before and (b) after tensile shear testing. [Color figure can be viewed in the online issue, which is available at www.interscience.wiley.com.]

### 2D SAXS and 2D WAXS of isotropic PA6

Figure 4 shows the 2D SAXS patterns of differently annealed isotropic PA6 films before [Fig. 4(a–c)] and after [Fig. 4(d–f)] the mechanical tests. Figure 4(g–i) also shows the 2D WAXS patterns of the respective samples after mechanical failure. As expected, the SAXS patterns of the samples before mechanical testing were nonoriented and of circular symmetry. They showed an almost homogeneous distribution of scattered intensity in the angular region between $-155\pi$ and $+155\pi$ (Fig. 5, solid symbols). Stretching to mechanical failure had a different effect on the orientation of the SAXS patterns, depending on the temperature of annealing. The sample annealed at 120°C, which attained the highest $\varepsilon_{br}$ [Fig. 1(a)], displayed an oriented SAXS pattern of fiber symmetry [Fig. 4(d)]. Its azimuthal scan (Fig. 5, 120°C, open symbols) was a typical example of a four-point scattering diagram with a bimodal distribution of scattered intensity. There was a strong orientation in the direction of the applied stress. Interestingly enough, in the 2D WAXS pattern of this same sample [Fig. 4(g)], the two Debye rings had apparent isotropic intensity distribution. Azimuthal scans in the $-155\pi/+155\pi$ angular region showed an almost isotropic internal ring ($\alpha$200) and some weak orientation in the external $\alpha$(002)/(202) ring coinciding with the stretching direction [Fig. 6(a)].

Annealing at 160°C caused the stretching of this sample to result in a much weaker orientation of the 2D SAXS pattern [Fig. 4(e)] compared to that of the

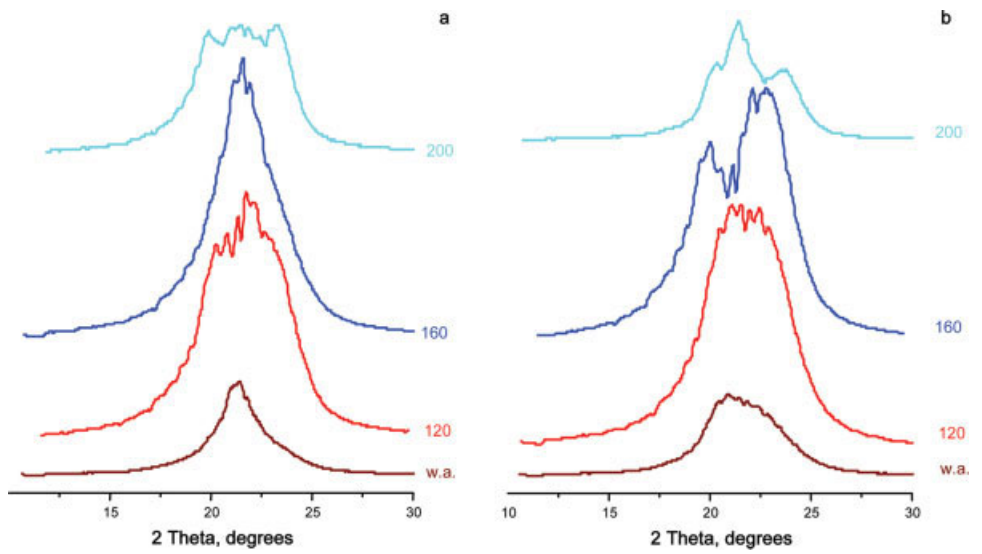


**Figure 3** 1D WAXS curves of oriented PA6 cables without annealing (w.a.) and with annealing for 1 h at different temperatures (a) before and (b) after tensile testing. [Color figure can be viewed in the online issue, which is available at www.interscience.wiley.com.]

**TABLE II**
**Crystallinity Data of the Variously Annealed Isotropic and Oriented PA6 Samples**

| Sample | Annealing temperature and time | $\alpha_{200}$ (%) | $\alpha_{002}/\alpha_{202}$ (%) | $\alpha$-CI (%) | $\gamma_{001}$ (%) | $\gamma_{200}$ (%) | $\gamma$-CI (%) | $CI_{Total}$ (ECI) | $\alpha/\gamma$ content |
|---|---|---|---|---|---|---|---|---|---|
| Isotropic PA6 | 120°C for 1 h | 17 (20) | 21 (28) | 38 (48) | 4 (2) | 2 (2) | 6 (4) | 44 (52) | 6.3 (12) |
| Isotropic PA6 | 160°C for 1 h | 17 (16) | 22 (25) | 39 (41) | 4 (5) | 2 (2) | 6 (7) | 45 (48) | 6.5 (6.0) |
| Isotropic PA6 | 200°C for 1 h | 14 (12) | 23 (29) | 37 (41) | 4 (3) | 2 (4) | 7 (7) | 44 (48) | 5.3 (5.8) |
| Oriented PA6 | No annealing | 5 (15) | 7 (17) | 12 (32) | 24 (8) | 9 (8) | 33 (16) | 45 (48) | 0.4 (2.0) |
| Oriented PA6 | 120°C for 1 h | 17 (18) | 13 (27) | 30 (44) | 2 (7) | 17 (2) | 20 (9) | 50 (53) | 1.5 (4.9) |
| Oriented PA6 | 160°C for 1 h | 17 (11) | 25 (30) | 42 (40) | 4 (5) | 2 (1) | 6 (6) | 48 (46) | 7.0 (6.7) |
| Oriented PA6 | 200°C for 1 h | 16 (11) | 20 (19) | 36 (30) | 4 (16) | 10 (9) | 14 (25) | 50 (55) | 2.6 (1.2) |

The numbers in parenthesis are the respective values after mechanical failure of the corresponding sample. For the isotropic samples, $CI_{Total}$ is the total crystallinity index representing the sum of the amounts of the $\alpha$ and $\gamma$ polymorphs. In the oriented samples, ECI accounted for the intensity of the equatorial PA6 reflections without the meridional 020 reflections.

previous sample. The difference of the azimuthal distribution of the scattered intensity between the initial unstressed and the broken samples was quite small (Fig. 5). At the same time, the anisotropy of the $\alpha(002)/(202)$ WAXS refection [Fig. 6(b)] was significantly stronger than the broken sample annealed at 120°C, which indicated a higher deformation of the crystalline phase. Similar effects were observed with the 2D SAXS and WAXS patterns of the sample annealed at 200°C and stretched to break [Fig. 4(f,i)]. As shown in the corresponding azimuthal scans in Figure 6, the anisotropy of the two WAXS reflections

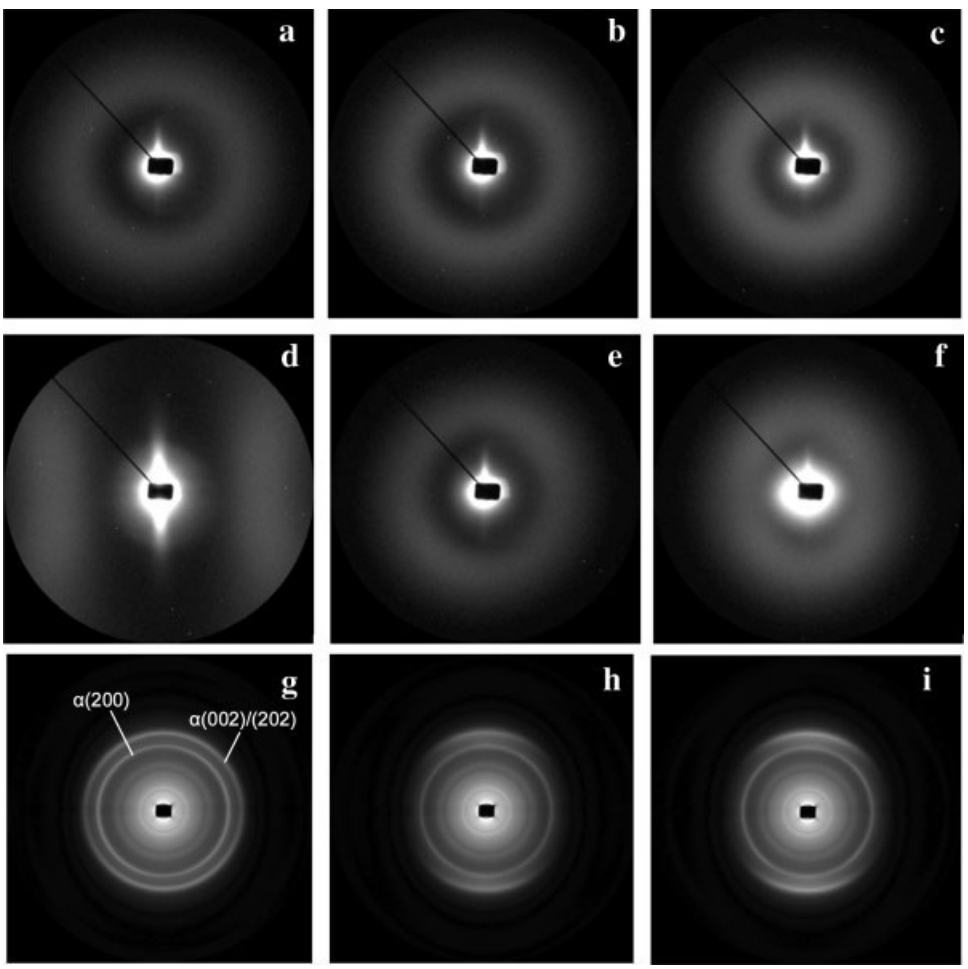


**Figure 4** 2D SAXS patterns of PA6 isotropic films annealed for 1 h at (a) 120, (b) 160, and (c) 200°C before tensile testing. (d–f) SAXS patterns of the same samples after testing. (g–i) 2D WAXS patterns of samples d–f.

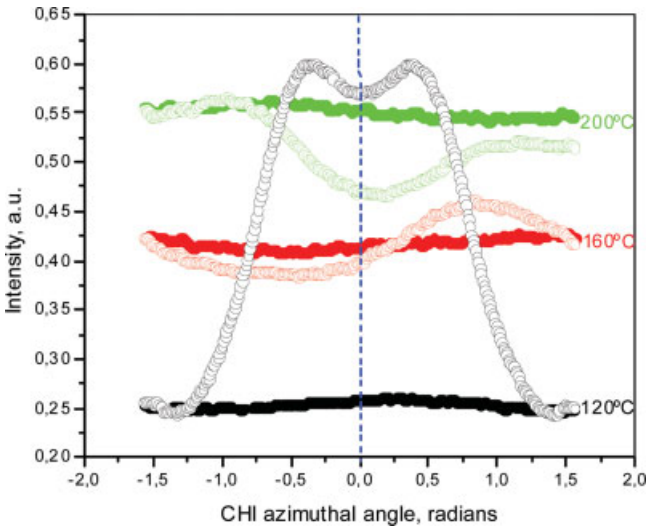


**Figure 5** Azimuthal scans in the −1.55 to +1.55 azimuthal angle (CHI) region (rad) of the 2D SAXS patterns of differently annealed isotropic PA6 films before (solid symbols) and after (open symbols) mechanical failure. [Color figure can be viewed in the online issue, which is available at www.interscience.wiley.com.]

were basically the same as those of the sample annealed at 160°C. The SAXS pattern after break of the film annealed at 200°C was slightly more anisotropic than that of the previous sample (Fig. 5).

Table III shows the evolution of the $L$ estimates of the isotropic PA6 samples as a function of the initial annealing temperature and stretching during the mechanical test. In the nondeformed samples, annealing at 200°C resulted in a clear growth of the $L$ values. The latter was due to an increase in the average amorphous phase thickness ($l_a$) to 36 Å, with the respective values at 120 and 160°C being 25 and 26 Å. At the same time, the average thickness of the crystalline domains ($l_c$) remained unchanged (67–68 Å). Mechanical failure of the samples annealed at 160 and 200°C resulted in a slight decrease of $l_c$, whereas the $l_a$ values increased so that the resulting $L$'s were slightly larger than those before the test. Only the isotropic sample annealed at 120°C, which after stretching showed an oriented 2D SAXS pattern, displayed a decrease in $L$ of almost 20 Å.

## 2D SAXS and 2D WAXS of data of oriented PA6

Table III also displays the $L$ values of all oriented cables before and after stretching. The Bragg long spacing obtained after Lorentz correction ($L_B$) values of the oriented cables annealed up to 160°C before mechanical testing remained relatively constant in the same range of 67–69 Å. The cable annealed at 200°C, however, displayed a larger $L_B$ of 88 Å. The stretching of all cables parallel to their fiber axis until failure resulted in slightly larger $L$'s, with the exception of the cable annealed at 200°C, which showed a smaller $L$. All of the oriented 2D SAXS patterns were very similar to those shown in Figure 7 obtained with a cable annealed for 1 h at 160°C before [Fig. 7(a)] and after [Fig. 7(b)] tensile testing. All cables showed typical two-point scattering diagrams with a streak in the central region.

The 2D WAXS patterns of differently annealed PA6 cables taken before and after tensile testing are presented in Figure 8. Here, the aforementioned increase in the α-form content that occurred as a result of annealing was best noticed in the sample heated for 1 h at 200°C before the tensile test [Fig. 8(d)], whereas the cable without annealing showed the most pro-

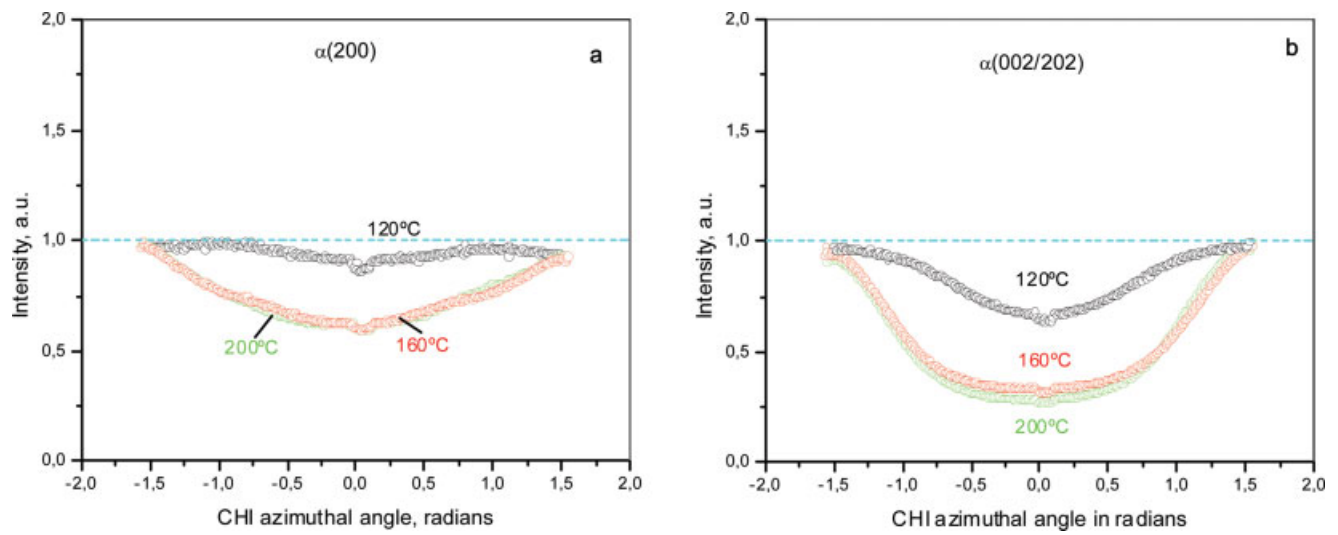


**Figure 6** Azimuthal scans in the −1.55 to +1.55 azimuthal angle (CHI) region (rad) of 2D WAXS patterns of differently annealed isotropic PA6 films after mechanical failure for the (a) inner α(200) reflection and (b) outer α(002/202) reflection. [Color figure can be viewed in the online issue, which is available at www.interscience.wiley.com.]

**TABLE III**
***L* Estimates for Differently Annealed Isotropic and Oriented PA6 Samples Before and After the Tensile Stress Test**

| | $L$ estimates (Å)[a] | | $l_c$ (Å) | | $l_a$ (Å) | |
|---|---|---|---|---|---|---|
| Annealing of 1 h | Before | After | Before | After | Before | After |
| Isotropic PA6 films | | | | | | |
| At 120°C | 90–92 | 71[b] | 67 | — | 25 | — |
| At 160°C | 91–94 | 97–98 | 68 | 63 | 26 | 34 |
| At 200°C | 101–105 | 103–107 | 67 | 64 | 36 | 41 |
| Oriented PA6 cable[b] | | | | | | |
| Without annealing | 68 | —[c] | — | | | |
| At 100°C | 67 | —[c] | — | | | |
| At 120°C | 66 | 70 | — | | | |
| At 160°C | 69 | 73 | — | | | |
| At 200°C | 88 | 82 | — | | | |

Before tensile testing, $l_c$ and $l_a$ were calculated from the linear CF.

[a] For the isotropic samples, $L$ estimates include $L_B$, $L_c^M$ (long spacing equal to the first maximum of linear CF), and $L_c^m$ (long spacing equal to twice the value of the first minimum of the linear CF) values.[10]

[b] For the oriented samples, $L_B$ values were obtained only after Lorentz correction and subtraction of the liquid scattering.

[c] The sample did not show coherent SAXS scattering.

nounced growth of the α-form content as a result of the tensile test [Fig. 8(e)]. As shown by the differences in the diffracted intensity, the cable without annealing [Fig. 8(e)] and that annealed at 120°C (8f) suffered serious damage in their crystalline structures caused by stretching. This damage was more evident than that in the cables annealed at 160 and 200°C [Fig. 8(g,h)]. Also, the (020) meridional pointlike reflections of the γ-PA6 were observable regardless of the fact that the content of this polymorph strongly decreased as a result of both annealing and stretching (Table II). The (020) reflections were used to calculate the *b* axis of the γ phase in all cables (Table IV). The rest of the *d*-spacings shown in Table IV were extracted from the corresponding 1D WAXS patterns as a function of the annealing temperature and stretching. They are considered in the Discussion section.

## DISCUSSION

### Isotropic PA6 films

If one analyzes the stress–strain curves in Figure 1(a) and the numeric data in Table I, it becomes evident that the higher the annealing temperature was, the higher the $E$ and $\sigma_y$ values were, with the engineering $\varepsilon_{br}$ decreasing from 80 to about 40%. At the same time, X-ray analysis showed that annealing did not significantly change the crystalline structure of the isotropic PA6 films. As shown in Table II, α-PA6 was the preferable crystalline form, independent of the annealing temperature. The α-form content varied in the range 37–39%, whereas the γ-form content was 6–7%. The data in Table III demonstrates that annealing changed neither $L$'s, nor the respective thicknesses of the crystalline and amorphous domains of the iso-

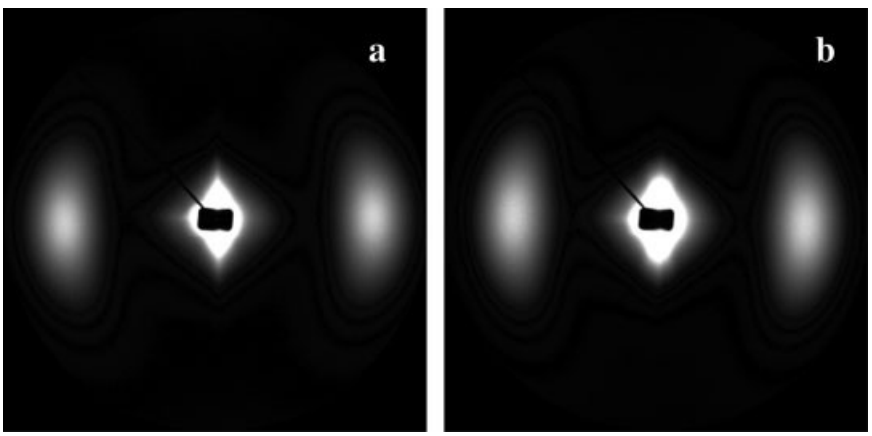


**Figure 7** Typical 2D SAXS patterns of oriented PA6 cables (a) before and (b) after tensile testing. Before testing, the sample was annealed for 1 h at 160°C.

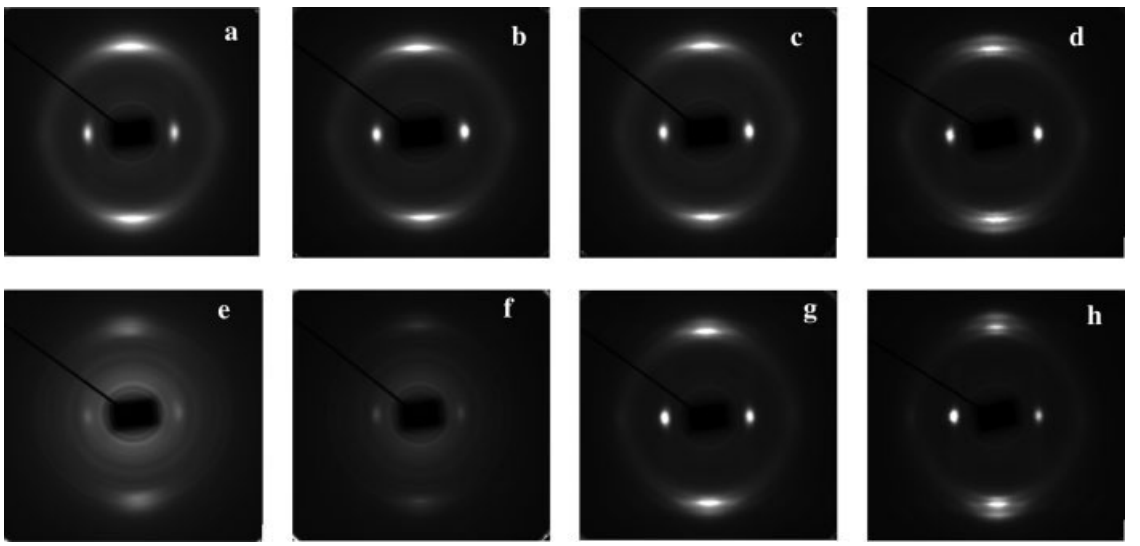


**Figure 8** 2D WAXS patterns variously annealed PA6 oriented cables before tensile testing: (a) without annealing, (b) annealing at 120°C, (c) annealing at 160°C, and (d) annealing at 200°C. (e–h) WAXS patterns of the same samples after tensile testing.

tropic PA6. Only annealing close to the Brill transition point (190–200°C) resulted in an increase in $L$ of about 10 Å, which was mainly due to the increase in $l_a$, whereas $l_c$ remained the same. Regardless of the fact that all the characteristics of the crystalline structure (degree of crystallinity, polymorph type, and lamellar and amorphous domain thicknesses) did not change significantly under annealing, the tested PA6 isotropic samples displayed different tensile behaviors. It is known that the changes in $E$ and $\sigma_y$ values can be related to the crystalline phase.[12] The PA6 plasticity in particular was found to be governed by the crystal slip parallel to the H-bonded sheets, that is, parallel to the (002) crystalline plane in the α form and to the (200) crystalline plane in the γ form, without breakage of the H bonds.[6,7,9] Therefore, $\sigma_y$ of PA6 was controlled, on the crystallographic level, by the intersheet distance of the two crystalline forms, which corresponded to the $d$-spacings of the above planes. As shown in Table IV, the intersheet distance of the α-type crystallite remained lower than that of the γ type within the entire annealing temperature range. Moreover, the increase in the annealing temperatures led to a decrease in the $d$(002) of the α form from 7,216 to 7.165 Å. Although the contribution of the γ form is very small (only 6–7% from the total CI), the $d$-spacing of the (200) plane in this polymorph also decreased from 7.675 to 7.640 Å. As a result, the critical resolved shear stress of the main sleep planes in both PA6 polymorphs became bigger at higher annealing temperatures and thus contributed to the $\sigma_y$ growth.

When we considered the 2D SAXS patterns in conjunction with the respective 2D WAXS images of the

**TABLE IV**
**Unit Cell Vectors and the Corresponding *d*-Spacings Obtained from the 1D WAXS Patterns of Isotropic and Oriented PA6 Samples as a Function of Their Initial Annealing Before and After the Tensile Test that Resulted in Sample Failure**

| | $d_{\alpha 200}$ | | $d_{\alpha 002/202}$ | | $d_{\gamma\ 200}$ | | $d_{\gamma\ 001}$ | | $d_{\gamma\ 020}$ | |
|---|---|---|---|---|---|---|---|---|---|---|
| Annealing of 1 h | Before | After | Before | After | Before | After | Before | After | Before | After |
| PA6 isotropic film | | | | | | | | | | |
| At 120°C | 8.499 | 8.465 | 7.216 | 7.314 | 7.675 | 7.808 | 3.990 | 4.008 | — | — |
| At 160°C | 8.522 | 8.566 | 7.197 | 7.187 | 7.682 | 7.649 | 4.011 | 4.002 | — | — |
| At 200°C | 8.558 | 8.554 | 7.165 | 7.138 | 7.640 | 7.671 | 4.100 | 4.054 | — | — |
| PA6 oriented cables | | | | | | | | | | |
| Without annealing | 8.610 | 8.453 | 7.467 | 7.544 | 7.800 | 7.828 | 4.080 | 4.105 | 16.858 | 15.300 |
| At 120°C | 8.342 | 8.418 | 7.438 | 7.633 | 7.928 | 7.826 | 4.074 | 4.038 | 15.880 | 15.300 |
| At 160°C | 8.522 | 8.566 | 7.197 | 7.187 | 7.682 | 7.649 | 4.011 | 4.002 | 16.028 | 14.640 |
| At 200°C | 8.558 | 8.554 | 7.165 | 7.138 | 7.640 | 7.671 | 4.100 | 4.054 | 16.028 | 14.400 |

The **b** vector of the γ form was obtained from the meridional (020) reflection (Fig. 8).

samples after tensile testing [Figs. 4(d–f) and 4(g−i), respectively], this allowed us a deeper insight into the relation between the structure and the mechanical properties of PA6 isotropic films. The α-form content and total CI of all samples after break increased by 2–10%; this was more notable in the sample annealed at 120°C (Table II). When considered that the γ-type crystallinity was almost constant, this increase could not be due to a phase transition but was probably a result of stress-induced crystallization of amorphous material into α-PA6, which was better expressed with the sample annealed at 120°C. The same sample displayed, after break, a high anisotropy of the SAXS pattern along the DR and a significant decrease in $L_B$ [Fig. 4(d), Fig. 5 (120°C), and Table III]. At the same time, in its WAXS pattern, the two Debye rings corresponding to the α(200) and α(002/202) reflections were entirely isotropic [Fig. 4(g)]. Evidently, annealing at 120°C resulted in a quite ductile PA6 film with an amorphous phase susceptible to crystallization. Stretching increased the α form/γ form proportion almost twice (Tab. 2), mainly at the expense of strain-induced crystallization. The amorphous regions were those that bore the stress, whereby a microfibrillar structure was formed with such an alignment of the crystalline domains that led to a decrease in the $L$ values.[13] As shown in Figure 4(g), these crystalline domains deformed very slightly, without a change in the almost isotropic distribution of the scattered intensity along the (α200) or α(002/202) reflection (Fig. 6).

Unlike the PA6 film annealed at 120°C, the samples treated at 160 and 200°C had SAXS patterns after stretching that were much more isotropic [Fig. 4(e,f) and Fig. 5], but the WAXS images showed more orientation along DR, especially of the outer α(002/202) reflection. As also shown in the respective 1D WAXS patterns in Figure 2, the sample annealed at 200°C suffered the strongest changes in its crystalline structure after break. We concluded that after annealing at 160 and 200°C, the external stress applied led to the deformation of the crystalline phase rather than to the deformation of the amorphous phase. It seems that annealing at elevated temperatures provoked a certain hardening of the amorphous domains that could not be accounted for by SAXS and WAXS but affected the deformability of the isotropic PA6. The existence of a harder (also called rigid) amorphous phase in the PA6 fibers was proven by solid state $^{13}$C-NMR and $^{1}$H-NMR.[14–16] Again, in the PA6 fibers, the presence of an oriented fraction in the amorphous phase has been discussed.[17,18] To the best of our knowledge, so far there have been no reports relating the changes in the mechanical properties of isotropic PA6 (e.g., $E$, stress, and strain values) to alterations in its amorphous structure on annealing, as suggested in this study.

**Oriented PA6 cables**

The stress–strain curves of all PA6 cables [Fig. 1(b)] were characterized by double yield, with the two $\sigma_y$ values increasing linearly with the annealing temperature (Table I). Another observation was a drop in the ductility as the annealing temperature increased. The biggest $\varepsilon_{br}$ and concomitant strain hardening was displayed by the sample without annealing, whereas the PA6 cables annealed above 160°C exhibited an almost brittle failure. As to the $E$ values, they were also affected by annealing: the higher the temperature was, the bigger $E$ was.

The explanation of the tensile behavior of the annealed PA6 cables was related to the alterations in their respective crystalline structure. As shown in Table II, the preferable crystalline modification for nonannealed cable was the γ form. On annealing, the γ-to-α form transition started; this was better expressed above 120°C. The α polymorph became the predominant crystalline form for cables annealed between 120 and 200°C. Table II also shows that ECI increased slightly (by 3–5%); this indicated that some formation of α-form crystals out of the amorphous material also occurred. The SAXS results showed that the γ-to-α phase transition and the additional crystallization did not result in alterations of Bragg's $L$'s when the annealing temperature was up to 160°C (Table III). Annealing in the 160–200°C range, however, caused a growth in the $L_B$ values of approximately 20 Å. It was not possible to determine the discrete contribution of the two thicknesses ($l_c$ and $l_a$) to the said growth because the linear CF was not applicable for samples with fibber symmetry. Because CI after annealing did not change significantly, the bigger $L_B$ after annealing at 200°C could hardly be related to $l_c$ growth due to lamellar thickening. Moreover, as shown in Table IV, the $d$-spacings of all planes decreased, which meant that the thermal expansion should also be excluded as a possible reason for the increase in $L_B$. We suppose, therefore, that some structural changes in the amorphous domains occurred during annealing at 200°C and the subsequent cooling to 30°C, which contributed to the $L_B$ change.

We are inclined to consider that the aforementioned γ-to-α form transition occurring on annealing was the main reason for the increase in $E$ and $\sigma_y$. The γ-PA6 polymorph was shown to be more ductile, whereas the α polymorph was characterized by a bigger tensile strength.[8,9] Because with the increase of the annealing temperature the α form became predominant, we expected that PA6 cables annealed at higher temperatures would display bigger $\sigma_y$ values, as was the case. From the point of view of crystal slip-governed plasticity, this behavior could be related to the decrease in the intersheet distance in the two crystalline forms when annealed. As shown in Table IV, the $d$-spacing

of the (002)/(202) crystalline plane, which corresponded to the intersheet distance of the α form, remained smaller than that of the respective plane (200) in the γ form for each annealing temperature. In addition, the said distance decreased from 7.467 to 7.165 Å for the α form and from 7.800 to 7.640 Å for the γ form when the annealing temperature was increased to 200°C. Annealing, therefore, as in the case of the PA6 isotropic films, increased the critical resolved shear stress of the main slip planes in both the α and γ polymorphs of oriented PA6 cable, which thus led to higher $\sigma_y$ and $E$ values.

With regard to the appearance of two yield points, this could not be unambiguously related to the crystal slips occurring in the respective γ-type and α-type crystallites. There will have always been a contribution by the amorphous phase, provided that the tensile tests were made at room temperature, that is, below the glass-transition temperature of the material. The PA6 isotropic films, however, were also tested at room temperature, and both α and γ polymorphs were also present. Nevertheless, the respective stress–strain curves showed different behaviors. In our opinion, the observed double yield was more likely related to the appearance of the oriented fraction in the amorphous phase rather than to the presence of two polymorphs. The presence of such an oriented fraction was proven in oriented PA6 fibers.[18] One may suppose that the cold drawing used for the preparation of the PA6 cables in our case also may have generated an inhomogeneous amorphous phase that could have had an impact on yielding.

The impact of stretching on the structure of the PA6 oriented samples was related to a clear, stress-induced γ-to-α transition. Interestingly, the latter depended on the annealing temperature. The stretching of the cables with no annealing or with 1 h of annealing at 120°C resulted in a very accentuated phase transition, whereas with annealing at 160°C, this trend became weaker and even inverted when annealing at 200°C was applied (Table II, Fig. 8). One may suppose that the amorphous phase had an important impact on the phase transitions in the crystalline domains. When it was more flexible, as in the case of cables without annealing or with 1 h of annealing at 120°C, the stress-induced crystalline modifications were more intense. On the contrary, when there was a hardening of the amorphous phase at higher annealing temperatures, this impeded the crystalline phase transitions. Most probably, this effect had to do with the effectiveness of the transfer of the external stress to the crystalline domains.

## CONCLUSIONS

The PA6 isotropic films obtained by the compression molding of granules were predominantly in the α crystalline form, whereas the γ form was the preferred form for PA6 cables obtained by extrusion and consequent cold-drawing. The annealing applied did not significantly change the crystalline structure of isotropic films but caused a γ-to- α form transition in the oriented cables. Both isotropic and oriented PA6 showed a growth in the $E$ and $\sigma_y$ values with increasing annealing temperature. This behavior was explained, on a crystallographic level, by a decrease in the $d$-spacing of the main crystal slip planes of the two polymorphs after annealing. The external stress applied led to additional γ-to-α form transitions in both the isotropic and oriented PA6 samples, whereby the higher the annealing temperature was, the weaker the inclination to the stress-induced transition was. This effect was attributed to the possibility of the formation of a hard fraction (PA6 films) or an oriented fraction (PA6 cables) in the amorphous phase.

## References


1. Aharoni, S. M. *n*-Nylons, Their Synthesis, Structure and Properties; Wiley: New York, 1997; p 316.
2. Denchev, Z.; Oliveira, M. J.; Carneiro, O. S. J Macromol Sci Phys 2004, 43, 143.
3. Denchev, Z.; Oliveira, M. J.; Mano, J. F.; Viana, J. C.; Funari, S. S. J Macromol Sci Phys 2004, 43, 163.
4. Galeski, A.; Argon, A. S.; Cohen, R. E. Macromolecules 1991, 24, 3945.
5. Galeski, A.; Argon, A. S.; Cohen, R. E. Macromolecules 1991, 24, 3953.
6. Lin, L.; Argon, A. S. Macromolecules 1992, 25, 4011.
7. Lin, L.; Argon, A. S. Macromolecules 1994, 27, 6903.
8. Ito, M.; Mizuochi, K.; Kanamato, T. Polymer 1998, 39, 4593.
9. Penel-Pierron, L.; Séguéla, R.; Lefebvre, J.-M.; Miri, V.; Defecher, C.; Jutigny, M.; Pabiot, J. J Polym Sci Part B: Polym Phys 2001, 39, 1224.
10. Dencheva, N.; Nunes, T.; Oliveira, M. J.; Denchev, Z. Polymer 2005, 46, 887.
11. Samon, J. M.; Schultz, J. M.; Hsiao, B. S. Polymer 2000, 41, 2169.
12. Schrauwen, B. A. G.; v. Breemen, L. C. A.; Spoelstra, A. B.; Govaert, L. E.; Peters, G. W. M.; Meijer, H. E. Macromolecules 2004, 37, 8618.
13. Stribeck, N. Presented at the Conference on X-ray Investigations of Polymer Structures (XIPS 2001), Dec 2001, Bielsko Biala, Poland.
14. Schreiber, R.; Veeman, W. S.; Gabriellse, W.; Arnauts, J. Macromolecules 1999, 32, 4647.
15. Litvinov, V. M.; Penning, J. P. Macromol Chem Phys 2004, 205, 1721.
16. Buda, A.; Demco, D. E.; Bertmer, M.; B. Blu1mich, B.; Litvinov, V. M.; Penning, J. P. J Phys Chem 2003, 107, 5357.
17. Murthy, N. S.; Minor, H.; Bednarczyk, C.; Krimm, S. Macromolecules 1993, 26, 1712.
18. Murthy, N. S.; Bray, R. G.; Correale, S. T.; Moore, R. A. F. Polymer 1995, 36, 3863.